Draft version July 9, 2026
Typeset using LaTeX default style in AASTeX631

Asteroseismology of the Low-Mass ZZ Ceti Star TIC 353727306 Using C/O-Core Models

Manqi Zhang [1,2] Jianning Fu [1,2,3] Jiayi Zhang [4] and Tianqi Cang [5]

[1] Institute for Frontiers in Astronomy and Astrophysics, Beijing Normal University, Beijing 102206, China
[2] School of Physics and Astronomy, Beijing Normal University, Beijing 100875, China
[3] Xinjiang Astronomical Observatory, Chinese Academy of Sciences, Urumqi 830011, Xinjiang, China
[4] Institut für Astronomie und Astrophysik, Eberhard Karls Universität Tübingen, Sand 1, 72076 Tübingen, Germany
[5] Department of Scientific Research, Beijing Planetarium, No.138 Xizhimenwai Street, Beijing, 100044, China

ABSTRACT

Pulsating white dwarfs provide valuable probes of the internal structures and evolutionary histories of compact stellar remnants. We present an asteroseismological analysis of the ZZ Ceti (DAV) white dwarf TIC 353727306 based on TESS photometry from Sector 58 and 85. The Fourier analysis reveals 14 independent pulsation requencies after excluding one combination frequency, including one complete and two incomplete $\ell = 1$ rotationally split triplets. The three identified triplets suggest a mean dipole-mode period spacing of $\Delta\Pi \approx 53$ s, which is used as a supplementary consistency check when comparing several local minima found in the coarse-grid search. We then fit the triplet central modes and the remaining independent pulsation modes with theoretical periods computed from a dense grid of White Dwarf Evolution Code (`WDEC`) models. The prefered seismic solution corresponds to a mass of $M_* = 0.500 \pm 0.002 M_\odot$, an effective temperature of $T_{\rm eff} \approx 12,100 \pm 42$K, and a hydrogen-layer mass fraction of $\log(M_{\rm H}/M_*) = -5.03 \pm 0.02$, placing the star near the blue edge of the DAV instability strip. This mass lies close to the lower limit for forming C/O-core DAVs through single-star evolution. The optimal model features a homogeneous C/O core with a central oxygen abundance of $X_{\rm O} = 0.70 \pm 0.03$. The absence of strong mode trapping suggests a relatively thick hydrogen envelope.

Keywords: white dwarfs; ZZ Ceti stars (DAVs); asteroseismology

1. INTRODUCTION

White dwarfs (WDs) represent the final evolutionary state of over 98% of stars in the Milky Way, preserving in their interiors the integrated history of nuclear burning, mixing, and mass-loss processes from previous evolutionary stages (Winget & Kepler 2008; Fontaine & Brassard 2008; Althaus et al. 2010; Iben et al. 1997; Córsico et al. 2019). They also serve as fossil records of the Milky Way's early history, providing important constraints for Galactic evolution studies and cosmochronology (Winget et al. 1987; Fontaine et al. 2001; Córsico et al. 2019). Among WDs, hydrogen-atmosphere pulsating white dwarfs—ZZ Ceti or DAV stars—locate in a narrow instability strip on the Hertzsprung–Russell diagram, spanning approximately $T_{\rm eff} \approx 12,270$–$10,850$ K (Gianninas et al. 2005, 2011; Van Grootel et al. 2013; Tremblay et al. 2015). Objects located near the blue edge of the instability strip are typically characterized by relatively simple pulsation spectra with fewer excited modes and shorter pulsation periods compared with cooler DAV stars (Hermes et al. 2017b; Cang et al. 2025). DAV stars exhibit nonradial g-mode pulsations, whose excitation has been attributed either to the classical κ–γ mechanism (Dolez & Vauclair 1981; Winget et al. 1982) or to convective driving (Brickhill 1991; Goldreich & Wu 1999), offering a unique opportunity to probe their internal structures through asteroseismology.

Asteroseismology of DAV stars allows precise determinations of stellar mass, chemical stratification, and core composition (see, e.g., Castanheira & Kepler 2008; Romero et al. 2012; Córsico et al. 2019). In particular, the mean period spacing of high-order g-modes is sensitive to the total stellar mass, while deviations from the asymptotic period spacing

Corresponding author: Jianning Fu
jnfu@bnu.edu.cn

can reveal details of the chemical transition zones and envelope masses (Bradley & Winget 1991; Córsico & Althaus 2006; Tassoul 1980). In rotating stars, multiplets due to frequency splitting provide a means to measure stellar rotation rates (Ledoux 1951). When multiple pulsation modes sampling different regions of the stellar interior are detected, their rotational splittings can also provide constraints on the radial dependence of the internal rotation profile, offering a potential probe of differential rotation in white dwarfs (Hermes et al. 2017a; Córsico et al. 2019). These capabilities make DAVs valuable laboratories for testing models of white dwarf formation and evolution (Córsico et al. 2019).

Low-mass DAVs with $M_* \lesssim 0.45$–$0.55\,M_\odot$ are rarely detected and reported. The stellar evolution theory predicts that single-star evolution produces C/O-core white dwarfs above ~ 0.5–$0.53 M_\odot$, while lower-mass WDs are typically helium-core remnants from binary evolution (Meng et al. 2008; Prada Moroni & Straniero 2009; Han et al. 2002; Althaus et al. 2013; Istrate et al. 2016). The discovery of a low-mass DAV with a C/O core therefore provides an important test case for the boundary between single-star and binary evolutionary channels.

The target of this study, TIC 353727306, was identified as a photometric variable using data from *Gaia* and the Zwicky Transient Facility (Guidry et al. 2021), and later classified as a DA white dwarf through Gaia photometry (Jiménez-Esteban et al. 2023), placing TIC 353727306 within the DAV instability strip. Together with the available high-cadence *TESS* photometry, this makes the star a suitable target for frequency extraction, mode identification, and asteroseismic modeling. The atmospheric parameters determined from Gaia photometry are $T_{\rm eff} = 11,222.6 \pm 130$ K and $\log g = 7.972 \pm 0.019$ (Jiménez-Esteban et al. 2023). To date, no dedicated asteroseismic study has been carried out for this star. With its observation data from the *TESS* mission, we are motivated to carry out a detailed asteroseismic analysis to probe its internal structure and refine its fundamental parameters.

In this work, we perform a detailed asteroseismological analysis of TIC 353727306. The paper is organized as follows: Section 2.1 summarizes the reduction of the corresponding *TESS* photometric data. In Section 2.2, we describe the extraction and analysis of pulsation frequencies. Section 3 presents the seismic modeling procedure, including mode identification and parameter optimization. Finally, Sections 4 and 5 interpret the results and highlight the main conclusions, respectively.

2. TESS PHOTOMETRIC OBSERVATIONS

TIC 353727306 is a white dwarf listed in the TESS Input Catalog, located at $\alpha_{\rm J2000} = 02^{\rm h}40^{\rm m}29.66^{\rm s}$ and $\delta_{\rm J2000} = 66°36'37.06''$, with $G = 15.58$ mag.

2.1. *Data reduction*

TIC 353727306 was observed by the TESS mission in nine sectors (18, 19, 25, 52, 58, 59, 78, 85, and 86). Among the available photometry, the ultra-short 20-s cadence data from Sector 58 show the lowest noise level and therefore serve as the primary dataset for our subsequent light-curve analysis. For the remaining sectors, we only consider those with comparably good data quality that introduce additional independent frequencies. Following this selection, only Sectors 58 and 85 are retained for our study. The target pixel files (TPFs) are retrieved from the Mikulski Archive for Space Telescopes (`MAST`).[1]

To optimize the photometric signal-to-noise ratio (SNR), we test a series of aperture masks for both selected sectors of data and find that a custom aperture containing three pixels yields the cleanest light curves in each case. Figure 1 presents the finding chart and the adopted aperture mask for Sector 58 (Xing et al. 2024)[2]. A cross-check with both the *Gaia* DR3 catalog and the International Variable Star Index (`VSX`) [3] confirms that no other known variable stars lie within 30″ of the target, ensuring that the extracted photometry has no heavy contamination from nearby sources.

After removing NaN values, we normalize the flux and apply a flattening procedure using a first-order polynomial filter over a window of 4321 data points (∼1 d). This choice of window length effectively removes instrumental long-term systematics while preserving intrinsic pulsation signals on timescales of minutes. Outliers exceeding 4.5σ are clipped, resulting in final light curves containing 116,994 and 106,320 data points for Sector 58 and 85, respectively.

2.2. *Frequency analysis*

The reduced TESS light curves are analyzed using `Period04` (Lenz & Breger 2005), with standard prewhitening and least-square fitting applied to extract frequencies, amplitudes, and phases. The detection threshold was determined

[1] https://archive.stsci.edu/missions-and-data/tess

[2] This work makes use of `tpfi`, publicly available at https://github.com/keyuxing/tpfi.

[3] https://www.aavso.org/vsx

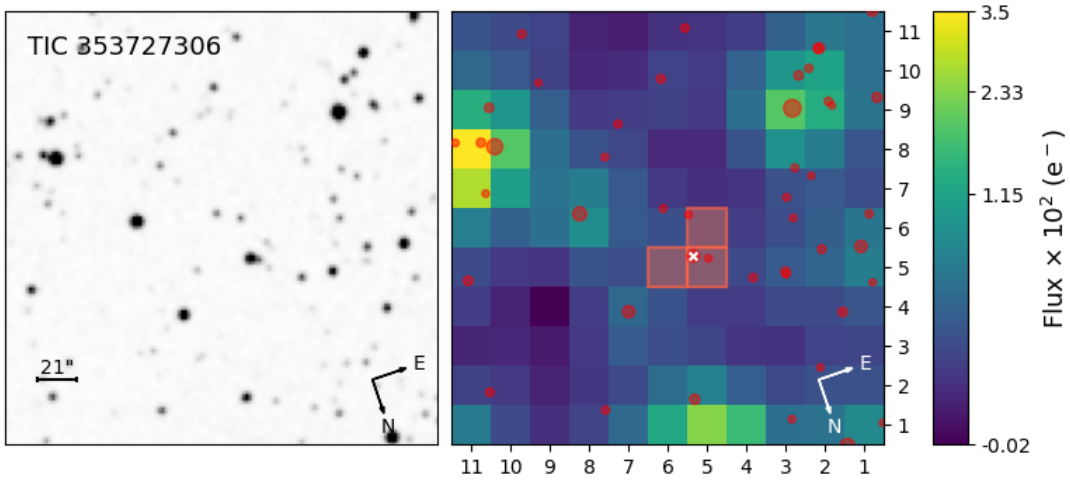

Figure 1. tpfi-generated finding chart and aperture mask for target TIC 353727306, optimizing photometric extraction.

from Monte Carlo simulations following the procedure described in Sect. 2.2 of Zong et al. (2016), yielding a significance level of 99% for S/N = 4.4 and above 99.99% for S/N > 5.1. Frequencies with S/N > 4.4 were therefore regarded as significant.

We identify 15 frequencies, including 14 independent frequencies and one linear combination frequency. Table 1 lists the frequencies derived from the `Period04` analysis. One complete triplet and two incomplete triplets are detected. The complete triplet exhibits an average frequency spacing of 37.176 μHz. In addition, each incomplete triplet shows two detectable components, which are interpreted as the $m = \pm 1$ side components of triplets. The Fourier amplitude spectrum obtained with `Period04` is shown in the upper panel of Figure. 2. Multiple significant peaks above the 4.4σ detection threshold are identified in Sector 58. The triplet structures are highlighted in the lower panels, with each component marked by red dots.

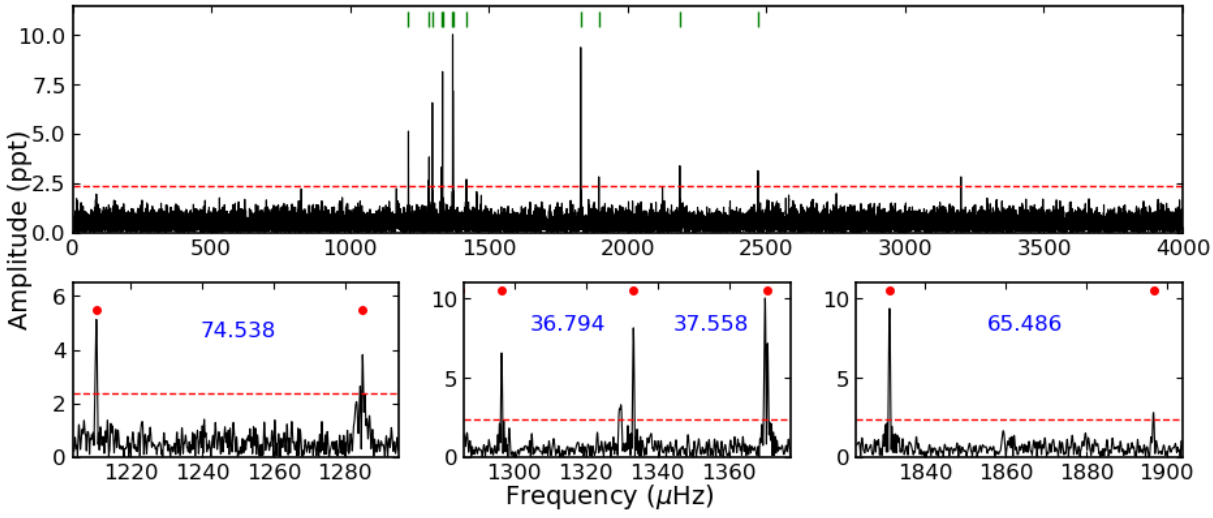

Figure 2. Top panel: Fourier amplitude spectrum of TIC 353727306 obtained with `Period04` for Sector 58. The horizontal red line indicates the 4.4 σ significance threshold, and the vertical short ticks mark the independent pulsation frequencies. Lower panels: Observed triplets and their measured frequency splittings.

Table 1. Frequencies derived for TIC 353727306 using the `Period04` software.

Name	Frequency (μHz)	σf (μHz)	Amplitude (ppt)	σA (ppt)	Period (s)	S/N	Sector	ID
f_1	1210.394	0.020	5.047	0.551	826.178	9.32	58	$f^*_{1,-1}$
f_2	1284.931	0.019	3.879	0.616	778.252	7.18	58	$f^*_{1,1}$
f_3	1296.539	0.025	6.539	0.550	771.284	12.09	58	$f_{2,-1}$
f_4	1329.815	0.028	3.442	0.858	751.984	6.36	58	
f_5	1333.333	0.012	8.187	0.672	750.000	15.13	58	$f_{2,0}$
f_6	1370.058	0.010	10.248	0.525	729.896	19.04	58	$f_{2,1}$
f_7	1370.891	0.015	6.534	0.563	729.452	11.86	58	
f_8	1419.398	0.036	2.687	0.532	704.524	4.97	58	
f_9	1673.704	0.037	3.646	0.584	597.477	5.49	85	
f_{10}	1831.192	0.010	9.385	0.609	546.092	17.39	58	$f^*_{3,-1}$
f_{11}	1896.678	0.035	2.827	0.566	527.238	5.23	58	$f^*_{3,1}$
f_{12}	2146.296	0.043	3.154	0.497	465.919	4.71	85	
f_{13}	2188.275	0.029	3.358	0.531	456.981	6.22	58	
f_{14}	2469.919	0.031	3.123	0.426	404.872	5.79	58+85	
f_{15}	3201.273	0.035	2.813	0.553	312.376	5.23	58	$f_6 + f_{10}$

NOTE—* The m identifications for the incomplete triplets are inferred from the observed rotational splitting pattern.

For adiabatic pulsations, the relationship between frequency splitting $\Delta\omega$ and rotational frequency Ω is given by:

$$\Delta\omega = m(1 - C_{l,n})\Omega, \tag{1}$$

where $C_{\ell,n}$ is the Ledoux constant, accounting for the Coriolis effect on pulsations. For high-order g-modes, $C_{\ell,n} \approx 1/[\ell(\ell+1)]$ (Ledoux 1951). Specifically, $C_{1,n} \approx 1/2$ for dipole modes and $C_{2,n} \approx 1/6$ for quadrupole modes. Based on the average splitting of 35.729 μHz for the three identified dipole triplets, we derive a rotational period of $P_{\rm rot} \approx 3.89$ hr. Although no quadrupole multiplet is observed, a theoretical splitting of 59.667 μHz is expected for $\ell = 2$ modes under the same rotation rate.

3. ASTEROSEISMOLOGICAL ANALYSIS

3.1. *Period-spacing identification*

The pulsation periods of white dwarfs are determined by their internal structure, making them sensitive probes of the stellar mass, effective temperature, and the thicknesses of the outer hydrogen and helium layers (Brassard et al. 1991). In the asymptotic limit, high-radial-order nonradial g-modes exhibit nearly constant period spacings that depend only on the spherical degree ℓ (Tassoul 1980; Tassoul et al. 1990). The asymptotic period spacing is given by

$$\Delta\Pi_\ell \approx \frac{\Delta\Pi_0}{\sqrt{\ell(\ell+1)}}, \tag{2}$$

where

$$\Delta\Pi_0 = 2\pi^2 \left(\int_{r_1}^{R} \frac{N}{r} dr \right)^{-1}. \tag{3}$$

Here N is the Brunt–Väisälä frequency and r is the radial coordinate.

Constraining the internal structure through asteroseismology normally requires reliable mode identification. However, only three rotationally split triplets are detected in the frequency spectrum of TIC 353727306, which is insufficient for a complete mode identification. We therefore search for constant period spacings using the Kolmogorov–Smirnov (K-S; Kawaler 1988), inverse variance (I-V; O'Donoghue 1994), and Fourier transform (F-T; Handler et al. 1997) significance tests[4], following the methodology of Su & Li (2023). Figure 3 shows the results for the three detected triplets. For the two incomplete triplets, the central ($m = 0$) components are not detected in the frequency spectrum. Assuming approximately symmetric rotational splitting, the central frequencies are estimated as the average of the two observed sidelobes. The corresponding periods are then used in the period-spacing analysis. The I-V test measures the inverse variance of the period distribution, with the maxima corresponding to constant spacings. The K-S test evaluates the uniformity of the period distribution, where the minima in the Q-statistic indicate systematic spacings. The F-T test computes the Fourier transform of Dirac-comb sampled periods, where peaks in frequency space indicate regular spacings. All three tests consistently detect a period spacing of $\Delta\Pi \approx 53$ s, which is interpreted as the dipole-mode ($\ell = 1$) period spacing. Because only three triplets are available, the remaining seven independent modes cannot be securely identified in terms of ℓ, m, or radial order n. Therefore, no further mode identification is attempted for these modes.

3.2. *Theoretical models setting*

We model carbon–oxygen (C/O) core white dwarfs using `MESA` (Paxton et al. 2011, 2013; Jermyn et al. 2023) and `WDEC` (Schwarzschild & Härm 1965; Bischoff-Kim & Montgomery 2018). In this procedure, `MESA` evolves zero-age main-sequence (ZAMS) progenitors to produce initial C/O cores, while `WDEC` constructs WD structures and computes adiabatic g-mode periods. The `WDEC` calculations are performed with version v20 (Bischoff-Kim & Montgomery 2018), which features a set of structural and microphysical control parameters, including the total mass ($M/M_\odot$), the effective temperature ($T_{\rm eff}$), the envelope base ($M_{\rm env}$), the envelope masses ($M_{\rm He}$, $M_{\rm H}$), the helium fraction in mixed layers ($X_{\rm He}$), the diffusion coefficients (α_1, α_2; Paquette et al. 1986; Thoul et al. 1994), the mixing length in the ML2/α flavour (Bergeron et al. 1995), and a parametric oxygen profile ($X_{\rm O}$) defined by break-point (height) parameters ($h_1 \geq h_2 \geq h_3$) and width parameters (w_1–w_4) to enforce monotonicity and mass-fraction control (Bischoff-Kim & Montgomery 2018; Salaris et al. 1997). This implementation yields physically consistent He/C/O stratification (deeper He penetration, extended O distribution), in closer agreement with evolutionary calculations (Salaris et al. 1997; Romero et al. 2012; Córsico et al. 2019).

Interfaced with `MESA` r22.11.1, `WDEC` v20 leverages updated equations of state and opacity/electron-transport modules (Jermyn et al. 2023), as well as modern implementations of nuclear reaction rates and energy generation (Timmes & Swesty 2000; Jermyn et al. 2021; Irwin 2004; Rogers & Nayfonov 2002; Saumon et al. 1995), low-T molecular opacities (Lederer & Aringer 2009; Marigo & Aringer 2009), Compton-scattering corrections (Poutanen 2017), and updated conductive opacities (Cassisi et al. 2007). The convection is treated with the mixing-length theory in the ML2/α calibration (Bergeron et al. 1995) and, where required for pulsation driving tests, a time-dependent convection

[4] Code available at https://github.com/keatonb/meanperiodspacing.

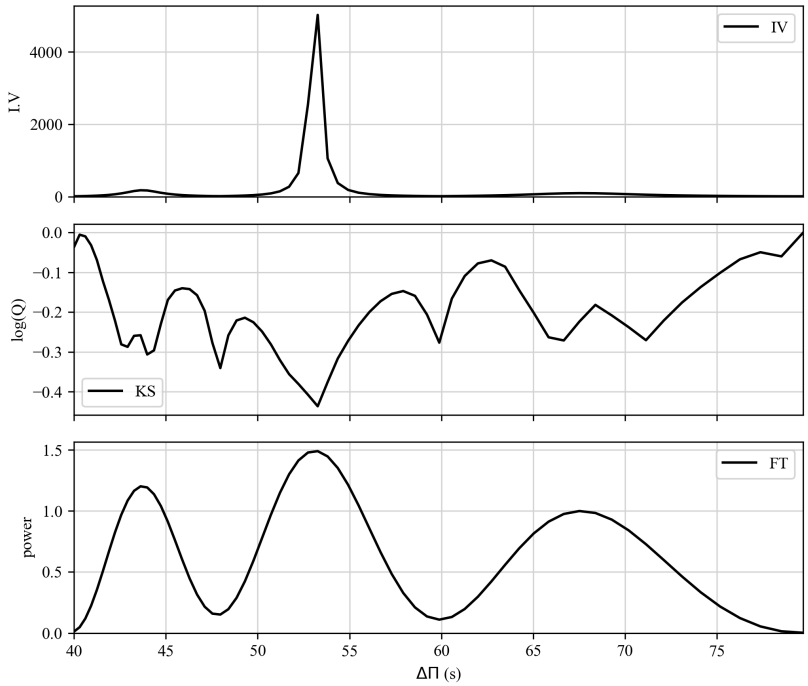

Figure 3. Significance tests for a constant period spacing in TIC 353727306. The upper, middle, and lower panels show the I-V, K-S, and F-T tests, respectively, applied to the three triplets listed in Table 1. All three tests consistently suggest a dipole ($\ell = 1$) period spacing of $\Delta\Pi_1 \approx 53$ s.

prescription (Brickhill 1991; Montgomery 2005). The chemical diffusion is solved following the multicomponent Burgers formalism with coefficients from Paquette et al. (1986) (see also Thoul et al. 1994).

Our forward modeling approach evaluates fit quality via the merit function

$$\chi^2 = \frac{1}{N}\sum_{i=1}^{N}(P_{\rm calc} - P_{\rm obs})^2 \tag{4}$$

with $P_{\rm calc}$ and $P_{\rm obs}$ denoting calculated/observed periods, respectively, N the mode count, and lower χ^2 values indicating superior matches between the theoretical model pulsation periods and the observed periods.

3.3. *Model matching*

Because only three rotationally split triplets are detected, a full mode identification is not feasible. Instead, we adopt a partially constrained fitting strategy. The three central components of the triplets are fixed as dipole modes ($\ell = 1$, $m = 0$), while the remaining seven independent frequencies are not assigned specific quantum numbers (ℓ, m, or n). These frequencies are therefore matched to theoretical modes without prior identification. In addition, the mean period spacing $\Delta\Pi \approx 53$ s derived from the triplets is included as an additional constraint on the model selection.

The core oxygen profile is initialized using parameters ($h_1 = 0.734$, $h_2 = 0.575$, $h_3 = 0.368$, $w_1 = 41.8$, $w_2 = 9.1$, $w_3 = 44.6$, $w_4 = 1$) derived from detailed evolutionary modeling of a $Z = 0.01$ progenitor star, as illustrated in Figure 4. Default mass-dependent values are derived from photometric estimates of $T_{\rm eff}$ and $\log g$ for TIC 353727306 using the asteroseismic fitting tool.[5] The resulting composition profiles are comparable to those from the `LPCODE` (Althaus et al. 2005, 2009, 2010). This evolutionary code includes time-dependent mixing with possible extra-mixing (Herwig et al. 1997), updated nuclear burning physics (Althaus et al. 2003), OPAL radiative opacities (Iglesias & Rogers 1996; Marigo & Aringer 2009) complemented by conductive opacities (Cassisi et al. 2007), neutrino energy-loss rates (Haft et al. 1994; Itoh et al. 1996), multi-regime equations of state (Magni & Mazzitelli 1979; Segretain et al. 1994), and diffusion effects influencing the envelope composition.

[5] Code available at https://github.com/kim554/asteroseismic_fitting/tree/master.

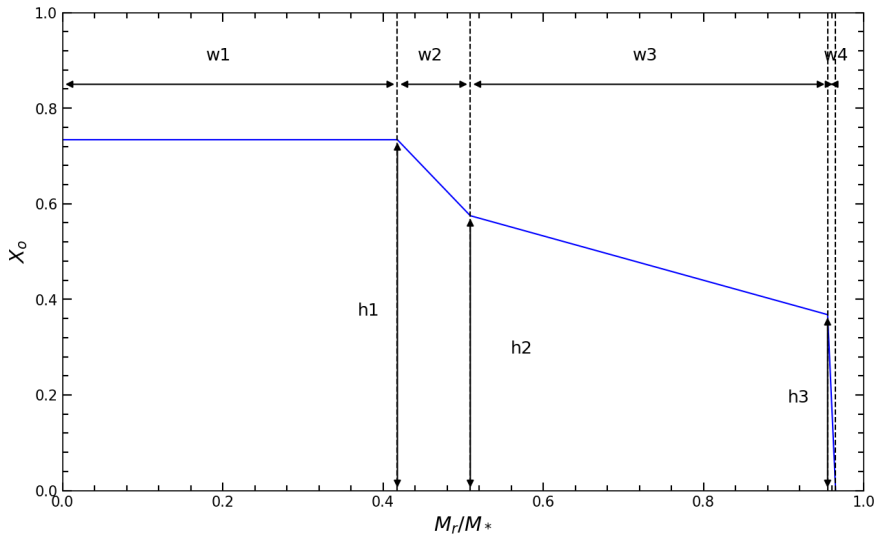

Figure 4. Parameterized oxygen abundance profile adopted as the initial core-composition profile for TIC 353727306.

A preliminary crude grid, constructed as listed in Table 2, is used to constrain the ranges of stellar parameters, while the central oxygen fraction $X_{\rm O}$ is allowed to vary dynamically during the optimization process. We adopt ML2/α = 1.25 for convection (Montgomery 2007; Koester 2010; Bergeron et al. 2011), and standard values of the diffusion coefficients α_1 and α_2. To account for possible rotational shifts, first-order Ledoux splitting corrections ($\pm\delta\omega$) are considered when comparing theoretical and observed frequencies.

Table 2. Parameter Ranges and Steps for the Crude and Fine Grids, respectively.

	Crude Grid		Fine Grid	
	Range	Step	Range	Step
$M/M_\odot$	[0.45,0.80]	0.05	[0.45,0.60]	0.005
$T_{\rm eff}$ [K]	[10600,12600]	250	[10600,12600]	50
$-\log(M_{\rm env}/M_*)$	[1.5,3]	1	[1.4,1.6]	0.01
$-\log(M_{\rm He}/M_*)$	[2,5]	1	[2.8,3.2]	0.01
$-\log(M_{\rm H}/M_*)$	[4,10]	1	[4.8,5.2]	0.01
$X_{\rm He}$	[0.05,0.9]	0.16	[0.1,0.2]	0.01
Initial $X_{\rm O}$ profile				
$h_1 = 73.4$	[50,80]	3	[65,75]	1
$h_2^* = 57.5$	[50,80]	3	[48,57]	1
$h_3^* = 36.8$	[20,41]	3	[25,34]	1
$w_1 = 41.8$	[25,60]	3	[36,48]	1
$w_2 = 9.1$	[1,20]	3	[3,15]	1
$w_3 = 44.6$	[30,48]	3	[39,51]	1
$w_4 = 1.0$	[1,5]	1	[1,3]	1

The crude-grid search produces several low-χ^2 candidate solutions spanning a range of stellar masses. To further constrain the models, we use the observed dipole-mode period spacing ($\Delta\Pi \approx 53$ s), derived from the three rotationally split triplets, as an additional seismic constraint. Figure 5 shows the asymptotic dipole-mode period spacings predicted by the lowest-χ^2 model at each stellar mass in the crude grid. Because the asymptotic period spacing depends sensitively on stellar mass, the observed period spacing favors the low-mass solutions, particularly those near $M_* \approx 0.50$–$0.60\,M_\odot$,

whereas higher-mass models generally predict substantially smaller period spacings. Guided by this constraint, we construct a fine grid centered on the preferred low-mass region ($M_* \approx 0.50\,M_\odot$) and carry out a refined search for the optimal model.

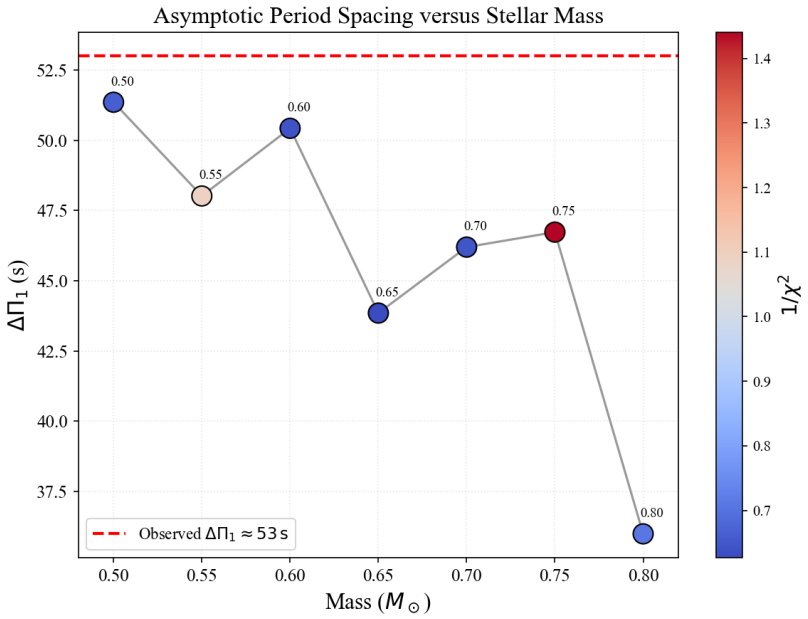

Figure 5. Dipole-mode asymptotic period spacings predicted by the lowest-χ^2 model at each stellar mass in the crude grid. The color scale denotes $1/\chi^2$, with warmer colors indicating better-fitting models. The dashed red line marks the observed dipole-mode period spacing, $\Delta\Pi_1 \approx 53$ s, derived from the three rotationally split triplets. The observed period spacing favors the low-mass solutions near $M_* \approx 0.50$–$0.60\,M_\odot$, which are subsequently explored with a fine-grid search.

We then compare the theoretical frequency sets with observed independent frequencies, and identify the prefered seismic solution by minimizing the merit function (Equation 4). The fine-grid search converged to a preferred seismic solution with $\chi^2 = 0.473$. Figure 6 (left panel) shows the distribution of $1/\chi^2$ in the $M/M_\odot$–$T_{\rm eff}$ plane, where warmer colors indicate better-fitting models. The right panel displays the corresponding internal chemical stratification and Brunt–Väisälä frequency of the preferred seismic solution.

Uncertainties of the derived parameter values are estimated following the approach of Zhang et al. (1986) and Romero et al. (2012). Our optimal seismic model yields $M_* = 0.500\,M_\odot$, $T_{\rm eff} \approx 12,100$ K, and a hydrogen layer mass of $\log(M_{\rm H}/M_*) = -5.03$. The preferred seismic solution also predicts a homogeneous C/O core extending to $M_r/M_* = 0.42$, with a central oxygen abundance of $X_{\rm O} = 0.70$. A summary of the optimal parameters is provided in Table 3, while Table 4 lists the calculated periods and quantum numbers (l, m, n) of all matched pulsation modes.

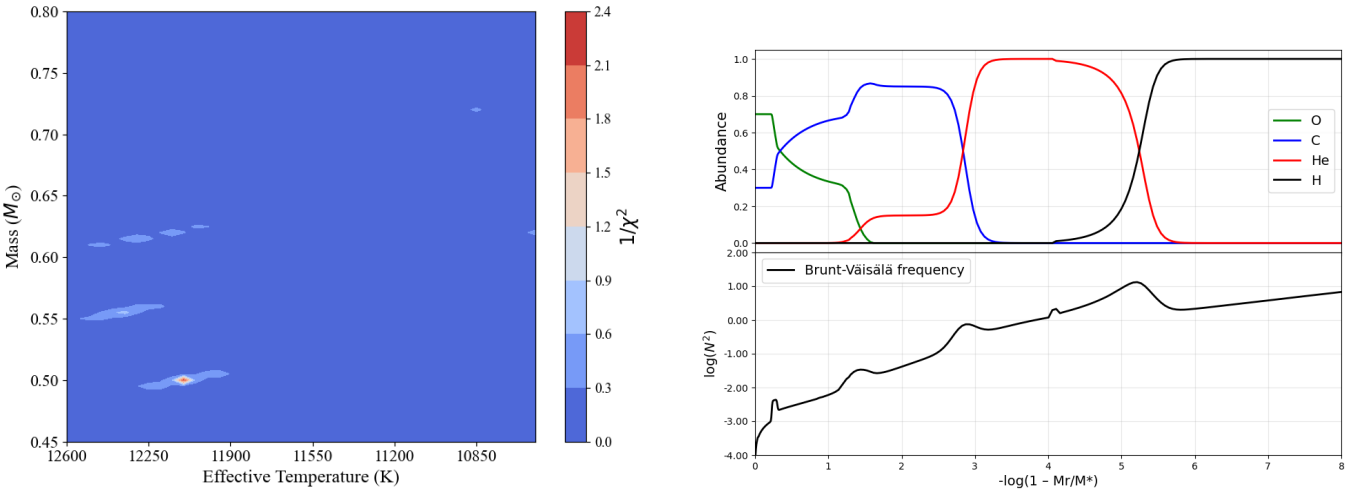

Figure 6. Left panel: Contours of $1/\chi^2$ on the $M_*/M_\odot$ versus $T_{\rm eff}$ plane. Right panel: Top—Chemical composition profiles of oxygen, carbon, and helium as a function of the fractional mass from the preferred seismic solution. Bottom—Logarithm of the squared Brunt-Väisälä frequency corresponding to the model.

Table 3. The optimal asteroseismological stellar parameters of TIC 353727306.

Parameters	Optimal
$M/M_\odot$	0.500 ± 0.002
$T_{\rm eff}$ [K]	$12,100 \pm 42$ K
$-\log(M_{\rm env}/M_*)$	1.52 ± 0.06
$-\log(M_{\rm He}/M_*)$	2.97 ± 0.04
$-\log(M_{\rm H}/M_*)$	5.03 ± 0.02
$X_{\rm He}$	0.15 ± 0.03
Initial $X_{\rm O}$ (%)	
$h_1 = 73.4$	70 ± 3
$h_2 = 57.5$	52 ± 4
$h_3 = 36.8$	31 ± 4
$w_1 = 41.8$	42 ± 1
$w_2 = 9.1$	9 ± 1
$w_3 = 44.6$	45 ± 1
$w_4 = 1.0$	1

Table 4. Mode identification and $P_{\rm obs}$ and $P_{\rm cal}$ derived from the preferred seismic solution.

l	m	n	$P_{obs}(s)$	$P_{cal}(s)$	$\lvert P_{obs} - P_{cal}\rvert(s)$	l	m	n	$P_{obs}(s)$	$P_{cal}(s)$	$\lvert P_{obs} - P_{cal}\rvert(s)$
2	2	11	404.872	404.574	0.298						
2	1	11		414.998							
2	0	11		425.973							
2	0	12	456.981	457.071	0.090						
2	2	13		453.792							
2	1	13	465.919	466.947	1.028						
2	0	13		480.888							
						1	1	7	527.238		
						1	0	7	536.499‡	535.526	0.973
						1	-1	7	546.092		
						1	1	9	597.477	598.690	1.213
						1	0	9		612.318	
2	0	21		717.888							
2	-1	21	751.984	751.377	0.607						
2	-2	21		788.142							
2	2	23	704.524	705.074	0.550						
2	1	23		737.351							
2	0	23		772.725							
2	2	24	729.452	728.920	0.532						
2	1	24		763.470							
2	0	24		801.459							
						1	1	12	729.896		
						1	0	12	750.000	750.106	0.106
						1	-1	12	771.284		
						1	1	13	778.252		
						1	0	13	801.499‡	801.058	0.441
						1	-1	13	826.178		
				χ^2						0.473	

Note—The double dagger symbol (‡) denotes periods derived from inferred central frequencies of rotationally split triplets. The central frequencies were estimated as the average of the two detected sidelobes, since the central components are not directly observed in the amplitude spectrum.

4. DISCUSSION

4.1. *Possible Evidence for Differential Rotation*

The three clearly identified $\ell = 1$ triplets provide important constraints on the internal rotation of TIC 353727306. As shown in Figure 2, the frequency separations between the multiplet components are not identical for the three modes. The average rotational splittings are 37.269 ± 0.014, 36.760 ± 0.013, and 32.743 ± 0.0180 μHz for the $k = 7$, 12, and 13 modes, respectively, suggesting a trend of decreasing rotational splitting with increasing mode frequency.

As will be discussed in Section 4.3, the period-spacing analysis suggests that mode trapping in TIC 353727306 is weak. Since mode trapping modifies the eigenfunctions and hence the rotational kernels (Kawaler et al. 1999), the resulting variations in the kernels are expected to be small and are unlikely to account for the observed differences in the splittings.

For adiabatic pulsations, the first-order rotational splitting is related to the stellar rotation rate through Equation (1), as derived under the perturbative treatment of slow rotation (Ledoux 1951). For $\ell = 1$ g-modes in white dwarfs, the Ledoux constant $C_{l,n}$ varies only weakly with radial order. Under the assumption of rigid rotation, different $\ell = 1$ modes are therefore expected to exhibit nearly identical frequency splittings. Using the average splitting of the three identified triplets, we derived a rotation period of approximately 3.89 hr. This value falls within the typical range observed for white dwarfs and pre-white dwarfs, spanning from about 1 hr to 18 days (Kawaler 2015; Hermes et al. 2017b; Córsico et al. 2019). However, it should be noted that this estimate assumes rigid-body rotation with a uniform angular velocity throughout the stellar interior.

The observed trend of smaller splittings at higher frequencies may indicate radial differential rotation.As shown in Figure 7, the rotational kernels of the three identified modes are broadly similar but not identical, with the $k = 7$ mode exhibiting a slightly greater sensitivity to the deeper interior than the higher-order modes.The possibility of probing radial differential rotation using rotational splittings has been explored in pulsating white dwarfs (e.g., Hermes et al. 2017a; Córsico et al. 2019).

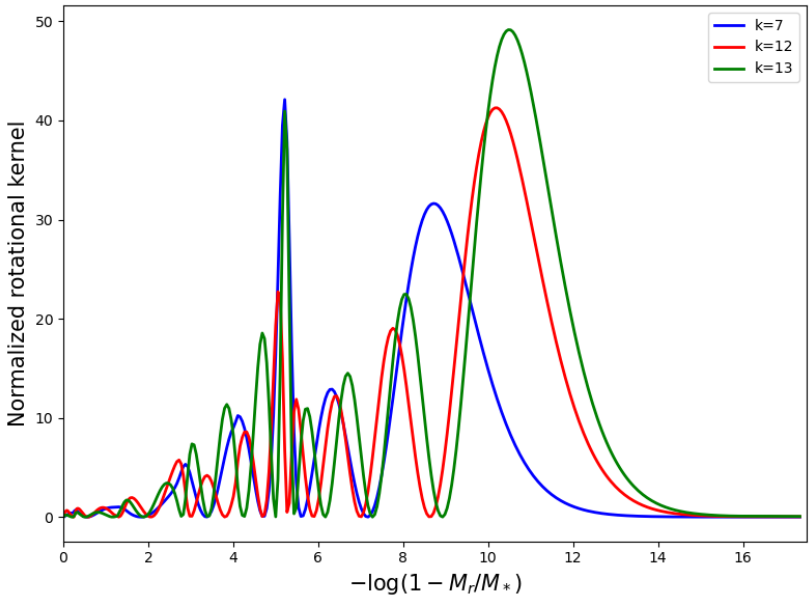

Figure 7. Normalized first-order rotational kernels for the three identified $\ell = 1$ modes ($k = 7$, 12, and 13) of the preferred seismic solution.

Given that only three triplets are currently detected, the available rotational information remains limited, and the evidence for differential rotation should therefore be regarded as tentative. Because TIC 353727306 is relatively faint ($m_G = 15.584$) and the TESS aperture is modest, the signal-to-noise ratio of the detected modes is limited, which restricts the precision of the measured frequency splittings. Higher-precision photometry from larger-aperture facilities will be required to place more stringent constraints on the internal rotation profile of TIC 353727306

4.2. *Low Mass and Blue-Edge Location of TIC 353727306*

In this section, we discuss two notable characteristics of the preferred seismic solution of TIC 353727306: its relatively low stellar mass and its location near the blue edge of the DAV instability strip.

Figure 8 presents the location of TIC 353727306 in the $T_{\rm eff}$–$\log g$ plane. The red triangle marks the position derived from our optimal asteroseismological model, while the green square shows the estimate based on Gaia photometry (Jiménez-Esteban et al. 2023). Previous non-seismic determinations collected from the literature are shown as black filled circles (Jiménez-Esteban et al. 2018; Gentile Fusillo et al. 2019; Xu et al. 2020; Guidry et al. 2021; Gentile Fusillo et al. 2021; Vincent et al. 2024; Madurga Favieres et al. 2024), while previously published asteroseismological results are indicated by black triangles (Romero et al. 2022, 2025). The background includes a sample of known DAV stars, where objects with published asteroseismological analyses are shown as light-blue circles and those without detailed seismic modeling as gray circles (Cang et al. 2025), respectively. The theoretical instability strip boundaries from (Tremblay et al. 2015) are indicated by blue and red dashed lines, together with DA white dwarf cooling tracks (black dashed lines).

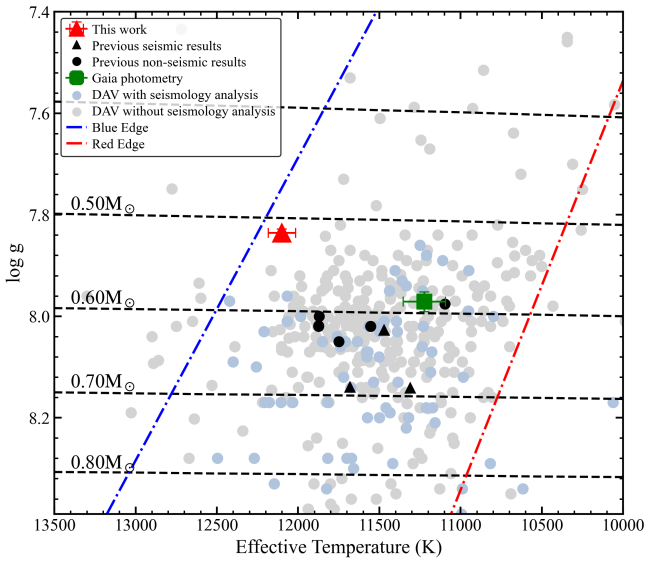

Figure 8. Location of TIC 353727306 in the $T_{\rm eff}$–$\log g$ plane. The red triangle with error bars shows our asteroseismological result, and the green square indicates the Gaia-based estimate (Jiménez-Esteban et al. 2023). Black circles and triangles represent previous non-seismic and asteroseismological results, respectively. Light-blue and gray circles show DAV stars with and without published seismic analyses. The theoretical instability strip and DA cooling tracks are also shown.

The asteroseismological solution places TIC 353727306 close to the theoretical blue edge of the DAV instability strip. Its pulsation properties are broadly consistent with expectations for hot DAV stars. Observational studies have shown that such objects typically exhibit relatively simple pulsation spectra with fewer excited modes than their cooler counterparts (Greiss et al. 2014; Hermes et al. 2017b; Chen et al. 2019). Consistent with this empirical trend, TIC 353727306 exhibits only three clearly detected rotationally split $\ell = 1$ triplets and a limited number of intrinsic $m = 0$ modes.

In addition to its location near the blue edge, TIC 353727306 is also remarkable for its unusually low seismic mass. Our preferred seismic solution yields a stellar mass of $0.500 \pm 0.002 M_{\odot}$, the lowest among all previous works. To assess the reliability of our seismic mass determination, we compare the theoretical forward period spacings computed from the adopted WDEC model with the observed pulsation periods. The resulting asymptotic period spacings are $\Delta\Pi_1 = 51.87$ s and $\Delta\Pi_2 = 30.24$ s, consistent with the observed mode distribution. This agreement provides a useful consistency check on the low-mass seismic solution, as the period spacing is sensitive to the stellar mass in pulsating white dwarf models (Córsico & Althaus 2006; Tassoul 1980).

Among previously studied DAVs, those with seismic masses below $0.505 M_{\odot}$ are extremely rare (Romero et al. 2012; Castanheira & Kepler 2008, 2009). The preferred C/O-core seismic model for TIC 353727306 exhibits a homogeneous

C/O-core structure, placing it near the lower-mass limit for single-star C/O WD formation (Meng et al. 2008; Prada Moroni & Straniero 2009).

4.3. *Mode Trapping*

Mode trapping occurs when the resonant phenomenon happens within a chemical transition zone, such as the interface between the hydrogen and helium layers in a DAV star. In such cases, the mode becomes confined or "trapped" in the outer layer, leading to a reduced amplitude in the stellar core and observable deviations from uniform period spacing (Bradley & Winget 1991). This effect is commonly diagnosed via period-spacing diagrams (ΔP vs. P); trapped modes appear as local minima and help constrain the hydrogen-layer mass and transition-zone depths (Bradley et al. 1993).

We compute the forward period spacings as

$$\Delta P_k = P_{k+1} - P_k, \tag{5}$$

and present the results in Fig. 9. The preferred seismic solution exhibits nearly uniform period spacings for both $l = 1$ and $l = 2$ modes with only minor fluctuations. No sharp or recurrent minima are detected, suggesting weak mode trapping. This supports the interpretation that the hydrogen envelope in this DAV star is relatively thick, which suppresses strong trapping signatures at composition gradients (Brassard et al. 1992).

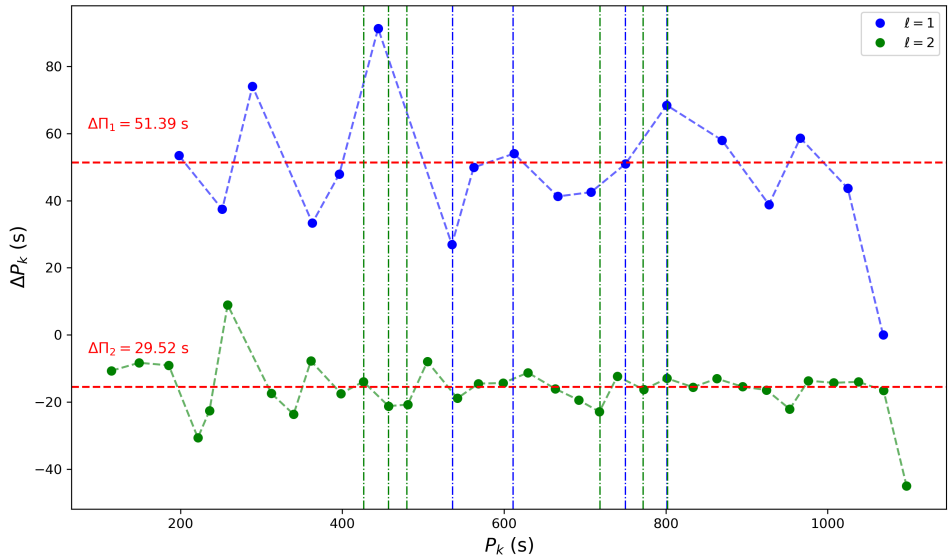

Figure 9. Period spacing diagram for TIC 353727306, The $\ell = 2$ sequence is vertically offset by 45 s for clarity.

4.4. *Comparison with Gaia Distance*

Finally, we compare the seismic solution with the Gaia DR3 measurements of TIC 353727306 (Bailer-Jones et al. 2021). With the apparent magnitude $m_G = 15.584 \pm 0.001$ mag and the distance $d_{\rm Gaia} = 56.547^{+0.126}_{-0.105}$ pc, we derive bolometric corrections from synthetic DA model grids[6] and find negligible extinction ($A_G \approx 0$ mag) at this distance using the Bayestar19 dust model (Green et al. 2019).

Following the method described by Bailer-Jones et al. (2018), the seismic luminosity is first converted into the absolute bolometric magnitude through

$$M_{\rm bol} = M_{\rm bol,\odot} - 2.5 \log \left(\frac{L}{L_\odot} \right), \tag{6}$$

where $M_{\rm bol,\odot} = 4.74$ mag is the solar bolometric magnitude. The absolute Gaia G-band magnitude is then obtained as

[6] http://www.astro.umontreal.ca/~bergeron/CoolingModels

$$M_G = M_{\rm bol} - BC_G. \tag{7}$$

The seismic distance is then calculated from the distance modulus,

$$m_G - M_G = 5\log\left(\frac{d_{\rm seismic}}{10\ {\rm pc}}\right) + A_G. \tag{8}$$

Using the seismic luminosity of $L = 3.85 \times 10^{-3}\,L_\odot$, we obtain a seismic distance of $d_{\rm seismic} = 65.92$ pc. The preferred seismic model yields a higher effective temperature and a lower stellar mass than the Gaia photometric estimates. Consequently, the luminosity predicted by the preferred seismic model corresponds to a seismic distance about 17% larger than the Gaia parallax distance. This discrepancy likely reflects the model dependence of the seismic luminosity and the adopted bolometric correction, as well as systematic differences between atmospheric parameters inferred from Gaia photometry and those obtained from asteroseismic modeling. Given the small Gaia distance of TIC 353727306, interstellar extinction is expected to have a negligible effect. Future spectroscopic constraints and improved seismic models will help clarify the origin of this discrepancy.

5. SUMMARY AND CONCLUSIONS

We perform a detailed asteroseismological analysis of the DAV star TIC 353727306 using high-quality TESS photometry from Sectors 58 and 85. Fourier analysis reveals 14 independent pulsation modes, including one complete and two incomplete $\ell = 1$ triplets. Assuming symmetric rotational splitting, the central components of the incomplete triplets are inferred and incorporated into the seismic analysis. The identified triplets yield a mean dipole-mode period spacing of approximately $\Delta\Pi_1 \approx 53$ s, which serves as an constraint for the model selection.

Using a series grid of WDEC models, we perform asteroseismic fitting to the observed pulsation periods. Our preferred seismic solution has a stellar mass of $M_* = 0.500 \pm 0.002\ M_\odot$, an effective temperature of $T_{\rm eff} = 12\,100 \pm 42$ K, and a hydrogen-layer mass fraction of $\log(M_{\rm H}/M_*) = -5.03 \pm 0.02$. The optimal model contains a homogeneous C/O core extending to $M_r/M_* \approx 0.42$ with a central oxygen abundance of $X_{\rm O} \approx 0.70$. The observed dipole-mode period spacing is consistent with the theoretical asymptotic value predicted by the preferred seismic solution, providing a useful consistency check on the adopted seismic solution. The identified triplets imply a mean rotation period of approximately 3.89 hr. Small but systematic differences among the measured rotational splittings may further hint at radial differential rotation, although additional multiplets and higher-precision observations are required to verify this possibility. In addition, the period-spacing diagram shows only weak deviations from uniform spacing, indicating weak mode trapping and suggesting the presence of a relatively thick hydrogen envelope.

TIC 353727306 is particularly interesting because its seismic mass lies close to the lower-mass boundary for the formation of C/O-core white dwarfs through single-star evolution. The star is also located near the blue edge of the DAV instability strip, where relatively simple pulsation spectra are expected. The three triplets provide valuable seismic constraints on its internal structure and rotation. The preferred C/O-core seismic solution, together with the low stellar mass and identifiable rotational multiplets, makes TIC 353727306 an important target for testing white dwarf evolutionary models near the transition between single-star and binary evolutionary channels. Future photometric observations will help further constrain the pulsation spectrum and internal rotation profile of this rare low-mass DAV star.

6. ACKNOWLEDGMENTS

JNF acknowledges the support from the National Natural Science Foundation of China (NSFC) through the grants 12427804 and 12273002. This work is supported by the China Manned Space Program with grant no. CMS-CSST-2025-A13, the Tianchi Talent Introduction Plan, and the Central Guidance for Local Science and Technology Development Fund under No. ZYYD2025QY27. TQC acknowledges the support from NFSC through the grants 12503035 and sponsored by Beijing Nova Program (202604841350). The authors thank Weikai Zong for valuable comments and suggestions that helped improve this manuscript. This research has made use of the SIMBAD database, operated at CDS, Strasbourg, France. The authors gratefully acknowledge the TESS team and all those who have contributed to making this mission possible. Funding for the TESS mission is provided by NASA's Science Mission Directorate.

REFERENCES

Althaus, L. G., Córsico, A. H., Bischoff-Kim, A., et al. 2010, ApJ, 717, 897, doi: 10.1088/0004-637X/717/2/897

Althaus, L. G., Miller Bertolami, M. M., & Córsico, A. H. 2013, A&A, 557, A19, doi: 10.1051/0004-6361/201321868

Althaus, L. G., Panei, J. A., Miller Bertolami, M. M., et al. 2009, ApJ, 704, 1605, doi: 10.1088/0004-637X/704/2/1605

Althaus, L. G., Serenelli, A. M., Córsico, A. H., & Montgomery, M. H. 2003, A&A, 404, 593, doi: 10.1051/0004-6361:20030472

Althaus, L. G., Serenelli, A. M., Panei, J. A., et al. 2005, A&A, 435, 631, doi: 10.1051/0004-6361:20041965

Bailer-Jones, C. A. L., Rybizki, J., Fouesneau, M., Demleitner, M., & Andrae, R. 2021, AJ, 161, 147, doi: 10.3847/1538-3881/abd806

Bailer-Jones, C. A. L., Rybizki, J., Fouesneau, M., Mantelet, G., & Andrae, R. 2018, AJ, 156, 58, doi: 10.3847/1538-3881/aacb21

Bergeron, P., Wesemael, F., Lamontagne, R., et al. 1995, ApJ, 449, 258, doi: 10.1086/176053

Bergeron, P., Wesemael, F., Dufour, P., et al. 2011, ApJ, 737, 28, doi: 10.1088/0004-637X/737/1/28

Bischoff-Kim, A., & Montgomery, M. H. 2018, AJ, 155, 187, doi: 10.3847/1538-3881/aab70e

Bradley, P. A., & Winget, D. E. 1991, ApJS, 75, 463, doi: 10.1086/191539

Bradley, P. A., Winget, D. E., & Wood, M. A. 1993, ApJ, 406, 661, doi: 10.1086/172477

Brassard, P., Fontaine, G., Wesemael, F., & Hansen, C. J. 1992, ApJS, 80, 369, doi: 10.1086/191668

Brassard, P., Fontaine, G., Wesemael, F., Kawaler, S. D., & Tassoul, M. 1991, ApJ, 367, 601, doi: 10.1086/169655

Brickhill, A. J. 1991, MNRAS, 251, 673, doi: 10.1093/mnras/251.4.673

Cang, T., Zhang, J., Fu, J.-N., Zhao, H., & Zong, W. 2025, Journal of Astrophysics and Astronomy, 46, 81, doi: 10.1007/s12036-025-10106-3

Cassisi, S., Potekhin, A. Y., Pietrinferni, A., Catelan, M., & Salaris, M. 2007, ApJ, 661, 1094, doi: 10.1086/516819

Castanheira, B. G., & Kepler, S. O. 2008, MNRAS, 385, 430, doi: 10.1111/j.1365-2966.2008.12851.x

—. 2009, MNRAS, 396, 1709, doi: 10.1111/j.1365-2966.2009.14855.x

Chen, J., Fu, J., Niu, H., & Li, C. 2019, NewA, 73, 101276, doi: 10.1016/j.newast.2019.101276

Córsico, A. H., & Althaus, L. G. 2006, A&A, 454, 863, doi: 10.1051/0004-6361:20054199

Córsico, A. H., Althaus, L. G., Miller Bertolami, M. M., & Kepler, S. O. 2019, A&A Rv, 27, 7, doi: 10.1007/s00159-019-0118-4

Dolez, N., & Vauclair, G. 1981, A&A, 102, 375

Fontaine, G., & Brassard, P. 2008, Communications in Asteroseismology, 157, 177

Fontaine, G., Brassard, P., & Bergeron, P. 2001, PASP, 113, 409, doi: 10.1086/319535

Gentile Fusillo, N. P., Tremblay, P.-E., Gänsicke, B. T., et al. 2019, MNRAS, 482, 4570, doi: 10.1093/mnras/sty3016

Gentile Fusillo, N. P., Tremblay, P. E., Cukanovaite, E., et al. 2021, MNRAS, 508, 3877, doi: 10.1093/mnras/stab2672

Gianninas, A., Bergeron, P., & Fontaine, G. 2005, ApJ, 631, 1100, doi: 10.1086/432876

Gianninas, A., Bergeron, P., & Ruiz, M. T. 2011, ApJ, 743, 138, doi: 10.1088/0004-637X/743/2/138

Goldreich, P., & Wu, Y. 1999, ApJ, 511, 904, doi: 10.1086/306705

Green, G. M., Schlafly, E., Zucker, C., Speagle, J. S., & Finkbeiner, D. 2019, ApJ, 887, 93, doi: 10.3847/1538-4357/ab5362

Greiss, S., Gänsicke, B. T., Hermes, J. J., et al. 2014, MNRAS, 438, 3086, doi: 10.1093/mnras/stt2420

Guidry, J. A., Vanderbosch, Z. P., Hermes, J. J., et al. 2021, ApJ, 912, 125, doi: 10.3847/1538-4357/abee68

Haft, M., Raffelt, G., & Weiss, A. 1994, ApJ, 425, 222, doi: 10.1086/173978

Han, Z., Podsiadlowski, P., Maxted, P. F. L., Marsh, T. R., & Ivanova, N. 2002, MNRAS, 336, 449, doi: 10.1046/j.1365-8711.2002.05752.x

Handler, G., Pikall, H., O'Donoghue, D., et al. 1997, MNRAS, 286, 303, doi: 10.1093/mnras/286.2.303

Hermes, J. J., Kawaler, S. D., Bischoff-Kim, A., et al. 2017a, ApJ, 835, 277, doi: 10.3847/1538-4357/835/2/277

Hermes, J. J., Gänsicke, B. T., Kawaler, S. D., et al. 2017b, ApJS, 232, 23, doi: 10.3847/1538-4365/aa8bb5

Herwig, F., Bloecker, T., Schoenberner, D., & El Eid, M. 1997, A&A, 324, L81, doi: 10.48550/arXiv.astro-ph/9706122

Iben, Icko, J., Ritossa, C., & García-Berro, E. 1997, ApJ, 489, 772, doi: 10.1086/304822

Iglesias, C. A., & Rogers, F. J. 1996, ApJ, 464, 943, doi: 10.1086/177381

Irwin, A. W. 2004, doi: https://freeeos.sourceforge.net/

Istrate, A. G., Fontaine, G., Gianninas, A., et al. 2016, A&A, 595, L12, doi: 10.1051/0004-6361/201629876

Itoh, N., Hayashi, H., Nishikawa, A., & Kohyama, Y. 1996, ApJS, 102, 411, doi: 10.1086/192264

Jermyn, A. S., Schwab, J., Bauer, E., Timmes, F. X., & Potekhin, A. Y. 2021, ApJ, 913, 72, doi: 10.3847/1538-4357/abf48e

Jermyn, A. S., Bauer, E. B., Schwab, J., et al. 2023, ApJS, 265, 15, doi: 10.3847/1538-4365/acae8d

Jiménez-Esteban, F. M., Torres, S., Rebassa-Mansergas, A., et al. 2023, MNRAS, 518, 5106, doi: 10.1093/mnras/stac3382

—. 2018, MNRAS, 480, 4505, doi: 10.1093/mnras/sty2120

Kawaler, S. D. 1988, in Advances in Helio- and Asteroseismology, ed. J. Christensen-Dalsgaard & S. Frandsen, Vol. 123, 329

Kawaler, S. D. 2015, in Astronomical Society of the Pacific Conference Series, Vol. 493, 19th European Workshop on White Dwarfs, ed. P. Dufour, P. Bergeron, & G. Fontaine, 65, doi: 10.48550/arXiv.1410.6934

Kawaler, S. D., Sekii, T., & Gough, D. 1999, ApJ, 516, 349, doi: 10.1086/307087

Koester, D. 2010, Mem. Soc. Astron. Italiana, 81, 921

Lederer, M. T., & Aringer, B. 2009, A&A, 494, 403, doi: 10.1051/0004-6361:200810576

Ledoux, P. 1951, ApJ, 114, 373, doi: 10.1086/145477

Lenz, P., & Breger, M. 2005, Communications in Asteroseismology, 146, 53, doi: 10.1553/cia146s53

Madurga Favieres, C., Kissler-Patig, M., Xu, S., & Bonsor, A. 2024, A&A, 688, A168, doi: 10.1051/0004-6361/202347368

Magni, G., & Mazzitelli, I. 1979, A&A, 72, 134

Marigo, P., & Aringer, B. 2009, A&A, 508, 1539, doi: 10.1051/0004-6361/200912598

Meng, X., Chen, X., & Han, Z. 2008, A&A, 487, 625, doi: 10.1051/0004-6361:20078841

Montgomery, M. H. 2005, ApJ, 633, 1142, doi: 10.1086/466511

—. 2007, Communications in Asteroseismology, 150, 253, doi: 10.1553/cia150s253

O'Donoghue, D. 1994, MNRAS, 270, 222, doi: 10.1093/mnras/270.2.222

Paquette, C., Pelletier, C., Fontaine, G., & Michaud, G. 1986, ApJS, 61, 177, doi: 10.1086/191111

Paxton, B., Bildsten, L., Dotter, A., et al. 2011, ApJS, 192, 3, doi: 10.1088/0067-0049/192/1/3

Paxton, B., Cantiello, M., Arras, P., et al. 2013, ApJS, 208, 4, doi: 10.1088/0067-0049/208/1/4

Poutanen, J. 2017, ApJ, 835, 119, doi: 10.3847/1538-4357/835/2/119

Prada Moroni, P. G., & Straniero, O. 2009, A&A, 507, 1575, doi: 10.1051/0004-6361/200912847

Rogers, F. J., & Nayfonov, A. 2002, ApJ, 576, 1064, doi: 10.1086/341894

Romero, A. D., Córsico, A. H., Althaus, L. G., et al. 2012, MNRAS, 420, 1462, doi: 10.1111/j.1365-2966.2011.20134.x

Romero, A. D., Kepler, S. O., Oliveira da Rosa, G., & Hermes, J. J. 2025, ApJ, 984, 112, doi: 10.3847/1538-4357/adc113

Romero, A. D., Kepler, S. O., Hermes, J. J., et al. 2022, MNRAS, 511, 1574, doi: 10.1093/mnras/stac093

Salaris, M., Domínguez, I., García-Berro, E., et al. 1997, ApJ, 486, 413, doi: 10.1086/304483

Saumon, D., Chabrier, G., & van Horn, H. M. 1995, ApJS, 99, 713, doi: 10.1086/192204

Schwarzschild, M., & Härm, R. 1965, ApJ, 142, 855, doi: 10.1086/148358

Segretain, L., Chabrier, G., Hernanz, M., et al. 1994, ApJ, 434, 641, doi: 10.1086/174766

Su, J., & Li, Y. 2023, ApJ, 943, 113, doi: 10.3847/1538-4357/aca533

Tassoul, M. 1980, ApJS, 43, 469, doi: 10.1086/190678

Tassoul, M., Fontaine, G., & Winget, D. E. 1990, ApJS, 72, 335, doi: 10.1086/191420

Thoul, A. A., Bahcall, J. N., & Loeb, A. 1994, ApJ, 421, 828, doi: 10.1086/173695

Timmes, F. X., & Swesty, F. D. 2000, ApJS, 126, 501, doi: 10.1086/313304

Tremblay, P. E., Gianninas, A., Kilic, M., et al. 2015, ApJ, 809, 148, doi: 10.1088/0004-637X/809/2/148

Van Grootel, V., Fontaine, G., Brassard, P., & Dupret, M.-A. 2013, in Astronomical Society of the Pacific Conference Series, Vol. 479, Progress in Physics of the Sun and Stars: A New Era in Helio- and Asteroseismology, ed. H. Shibahashi & A. E. Lynas-Gray, 229

Vincent, O., Barstow, M. A., Jordan, S., et al. 2024, A&A, 682, A5, doi: 10.1051/0004-6361/202347694

Winget, D. E., Hansen, C. J., Liebert, J., et al. 1987, ApJL, 315, L77, doi: 10.1086/184864

Winget, D. E., & Kepler, S. O. 2008, ARA&A, 46, 157, doi: 10.1146/annurev.astro.46.060407.145250

Winget, D. E., van Horn, H. M., Tassoul, M., et al. 1982, ApJL, 252, L65, doi: 10.1086/183721

Xing, K., Zong, W., Silvotti, R., et al. 2024, ApJS, 271, 57, doi: 10.3847/1538-4365/ad2ddd

Xu, S., Lai, S., & Dennihy, E. 2020, ApJ, 902, 127, doi: 10.3847/1538-4357/abb3fc

Zhang, E. H., Robinson, E. L., & Nather, R. E. 1986, ApJ, 305, 740, doi: 10.1086/164288

Zong, W., Charpinet, S., Vauclair, G., Giammichele, N., & Van Grootel, V. 2016, A&A, 585, A22, doi: 10.1051/0004-6361/201526300